Proceedings of the Institution of Mechanical Engineers, Part G: Journal of Aerospace Engineering, Volume 222, Number 7, 939-949, 2008

A numerical investigation into the effect of engine bleed on performance of a single-spool turbojet engine

N U Rahman* and **J F Whidborne**
Dynamics Simulations and Controls Group, Cranfield University, Bedfordshire, UK

The manuscript was received on 9 June 2008 and was accepted after revision for publication on 30 July 2008.

DOI: 10.1243/09544100JAERO389

Abstract: A real time simulation model has been developed to investigate the effect of variable engine bleed on steady state and transient performance of a single-spool turbojet engine. The bleed air is to be used for flow control on the aerodynamic control surfaces of a tailless configuration such as the blended wing body aircraft. The engine simulation uses the inter-component volume method and runs in MATLAB/Simulink environment. Bleed effects were simulated both with and without the control of engine speed. Experimental data for the advanced micro turbine (AMT) Olympus single-spool turbojet engine was used to validate the simulation results. Under nominal bleed conditions, the results were accurate to within 5 per cent of experimental values. While for excessive engine bleeds the results were accurate to within 10 per cent. The effect of engine bleed location along the compressor length was also incorporated. A proportional + integral speed controller with slew rate limiting was implemented as an integral part of the model. The method presented here could be easily expanded for steady state and transient performance simulation of two and three spool turbojet/turbofan engines.

Keywords: turbojet simulation, component volume method, bleed flow, engine performance

1 INTRODUCTION

The use of the propulsion system for aircraft control is a subject of active research at Cranfield University; one of the research objectives is to evaluate the feasibility of this concept for the blended wing body (BWB) configuration. Although having unique aerodynamic performance advantages [**1**], the BWB aircraft suffers from stability and control problems due to the absence of a horizontal stabilizer. An effort is being made to augment these stability issues by use of an integrated propulsion/flight control concept. Integrated propulsion can be used for active flow control over the main lifting surface as well as trailing edge flaps. The blended wing configuration in particular has large root chords which causes thickening of the boundary layer and flow separation, especially at high angles of attack. Bleed air from the engine can be used here to re-energize the boundary layer thus delaying or minimizing flow separation [**2**].

In a propulsion controlled aircraft, the power plant is directly involved in the generation or modification of control forces and lift. Englar [**3**] conducted a series of experiments on jet flaps and circulation control trailing/leading edge devices for lift enhancement. It was reported that with circulation control, lift coefficients comparable to or better than most complex mechanical flap systems can be achieved [**3**].

Variable engine bleed can however adversely affect engine performance. It not only degrades engine efficiency but also alters its dynamics. The two control inputs that are generally used to change the state of the engine are fuel flow and nozzle area. If engine bleed is a variable, it starts affecting the steady state and transient operation of the engine and may render the flow or circulation control concept infeasible.

This paper presents the work on modelling of engine dynamics and its overall performance under variable bleed conditions. The approach followed is to model various engine subsystems using performance maps and then interlink each individual component to get an overall engine performance model. Two

**Corresponding author: Dynamics Simulations and Controls Group, Cranfield University, Building 83, Bedfordshire MK43 OAL, UK. email: n.ur-rahman@cranfield.ac.uk*

approaches were considered: the inter-component volume method [**4**] and the constraint satisfaction iterative method [**5**]. However, the inter-component volume method was eventually selected due to its real time performance and simplicity. Both open loop (fuel flow demand defined by user) and closed loop (fuel flow demand set by engine speed control) responses were simulated. The advanced micro turbine (AMT) Olympus single-spool turbojet engine [**6**] was selected as a test case. The simulation results were validated with data from bleed experiments conducted on the AMT Olympus engine at the University of Manchester [**7**].

2 THE ENGINE MODEL

In order to simulate a dynamic system, it is important to specify a set of minimum number of variables or states ($\boldsymbol{X}$) that completely define the system dynamics. An input vector ($\boldsymbol{u}$) establishes a means of controlling or changing the state of the system. For a single-spool turbojet system, as shown in Fig. 1, the compressor and turbine exit pressures [P_3, P_5] are important system states. If component efficiencies and exit pressures are known, temperatures at various engine stages of the engine can be calculated using thermodynamic relationships. Shaft rotational speed (N) is another important parameter that forms part of the state vector. The fuel flowrate (w_f) and nozzle area (A_n) were used to control the state of the system. Thus the state and control vectors are defined as follows

$$\boldsymbol{X} = (P_3, P_5, N) \quad \text{and} \quad \boldsymbol{u} = (w_\mathrm{f}, A_\mathrm{n})$$

2.1 Intake model

In this work, a static intake model was incorporated and the flow process was assumed to be adiabatic. With the free stream static pressure and temperature as (p_0, t_0) and Mach number (M), the total conditions (T_1, P_1) at the intake face can be calculated from reference [**8**]

$$\frac{T_1}{t_0} = 1 + \frac{\gamma - 1}{2} M^2 \tag{1}$$

$$\frac{P_1}{p_0} = \left(\frac{T_1}{t_0}\right)^{\gamma/(\gamma-1)} \tag{2}$$

The total temperature (T_1) represents the rise in temperature by bringing air molecules travelling at Mach number (M) to rest at the intake face. The total pressure at the intake face is a function of temperature ratio and is given by equation (2). Since no energy is added in the intake, the total temperature remains constant [**9**]. However, there is a loss in total pressure as the flow passes through the intake and this pressure loss is a measure of intake efficiency (η_I). Therefore, the intake exit conditions are

$$T_2 = T_1 \tag{3}$$

$$P_2 = \eta_\mathrm{I}(P_1) \tag{4}$$

For the AMT Olympus, the intake efficiency is assumed to be 1.0.

2.2 The AMT Olympus compressor model

Representative AMT Olympus engine compressor maps from reference [**10**] are shown in Fig. 2. These maps are a function of non-dimensional compressor speed ($N_\mathrm{c}^* = N/\sqrt{T_2/T_\mathrm{std}}$) and the non-dimensional/corrected mass flow ($w_\mathrm{c}^* = w_\mathrm{c}\sqrt{T_2/T_\mathrm{std}}/P_2/P_\mathrm{std}$). Using these definitions, the compressor pressure ratio and corrected speed ($P_3/P_2, N_\mathrm{c}^*$) were calculated using the compressor inlet conditions (T_2, P_2) and knowledge of the state vector, $\boldsymbol{X} = (P_3, P_5, N)$. A two-dimensional interpolation routine was used to get the corrected mass flow and efficiency ($w_\mathrm{c}^*, \eta_\mathrm{c}$) from the compressor maps. From reference [**8**], the compressor temperature

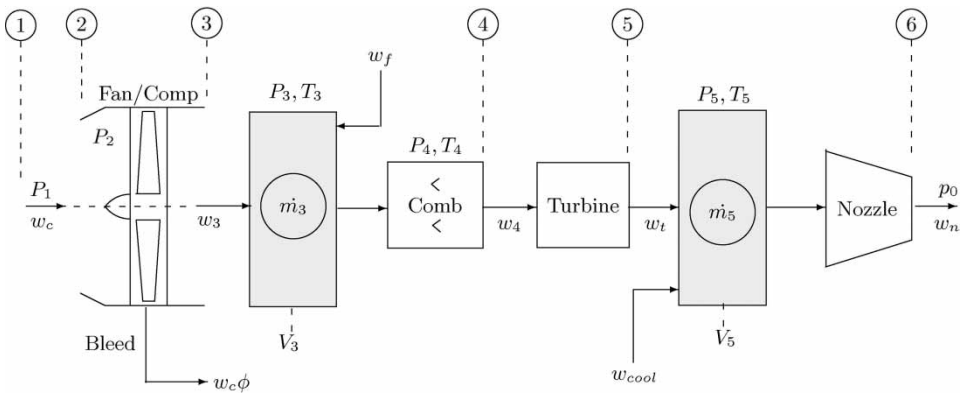

Fig. 1 Single-spool turbojet dynamic model with inter-component volumes

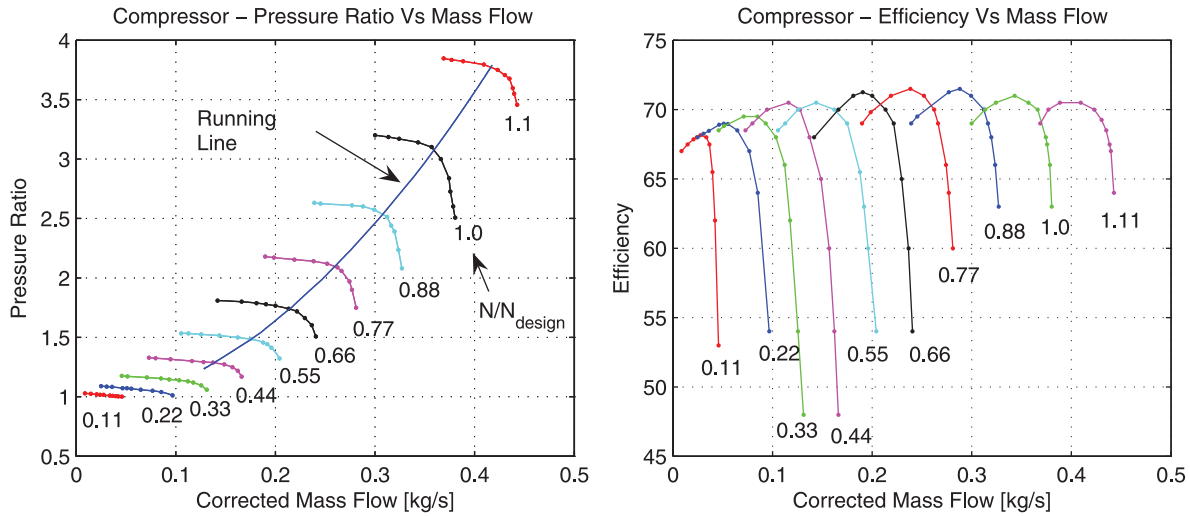

Fig. 2 Compressor map for the AMT Olympus engine

rise is

$$\Delta T_{23} = \frac{1}{\eta_c} T_2 \left[\left(\frac{P_3}{P_2} \right)^{(\gamma-1)/\gamma} - 1 \right] \tag{5}$$

The total temperature at the compressor exit is hence

$$T_3 = T_2 + \Delta T_{23} \tag{6}$$

If there is a fraction of bleed ($\phi = w_b/w_c$) taken from the compressor mass flow at a non-dimensional axial location (x/l) along the compressor, then the compressor exit mass flow is

$$w_3 = w_c(1 - \phi) \tag{7}$$

and keeping into account the bleed location (x/l), the torque required by the compressor is

$$\tau_{comp} = \frac{w_c c_p \Delta T_{23}}{N_{rad/s}} \left[(1 - \phi) + \phi \frac{x}{l} \right] \tag{8}$$

The above set of equations was used to calculate compressor exit conditions (w_3, T_3, P_3) and compressor torque, with inlet exit conditions (T_2, P_2) and the state vector, $\boldsymbol{X} = (P_3, P_5, N)$ as inputs.

2.3 The AMT Olympus combustor model

The AMT Olympus engine uses an annular type combustion chamber. The amount of energy imparted to the pressurized air depends upon the fuel to air ratio and the heating value (HV) of the fuel. Not all the fuel is burnt and a burner efficiency (η_b) is associated with the fuel burning process. A typical value for burning efficiency is 0.98. Reference [**11**] gives an expression for combustor temperature rise

$$\Delta T_{34} = \eta_b \left(\frac{w_f}{w_3} \right) \frac{HV_{fuel}}{c_p} \tag{9}$$

The combustor exit temperature is therefore

$$T_4 = T_3 + \Delta T_{34} \tag{10}$$

and the net mass flow from combustor

$$w_4 = w_3 + w_f \tag{11}$$

If the pressure loss (ΔP_{loss}) in the combustor is expressed as a fraction of the combustor entry pressure, the combustor exit pressure will be

$$P_4 = P_3(1 - \Delta P_{loss}) \tag{12}$$

This establishes the combustor exit conditions (w_4, T_4, P_4).

2.4 The AMT Olympus turbine model

Similar to the compressor, the turbine model for the AMT Olympus was also based on performance maps. The first map relates non-dimensional turbine mass flow ($w_t^* = w_t\sqrt{T_4}/P_4$) with turbine pressure ratio and the second map gives a measure of turbine efficiency. Representative turbine maps for the AMT Olympus turbojet engine from reference [**10**] are shown in Fig. 3. The speed line corresponding to lowest non-dimensional turbine speed ($N_t^* = N/\sqrt{T_4}$) is highlighted.

Using the state vector $\boldsymbol{X} = (P_3, P_5, N)$ and two-dimensional interpolation, the non-dimensional turbine mass flow and turbine efficiency (w_t^*, η_t) are calculated from the turbine maps. From reference [**8**],

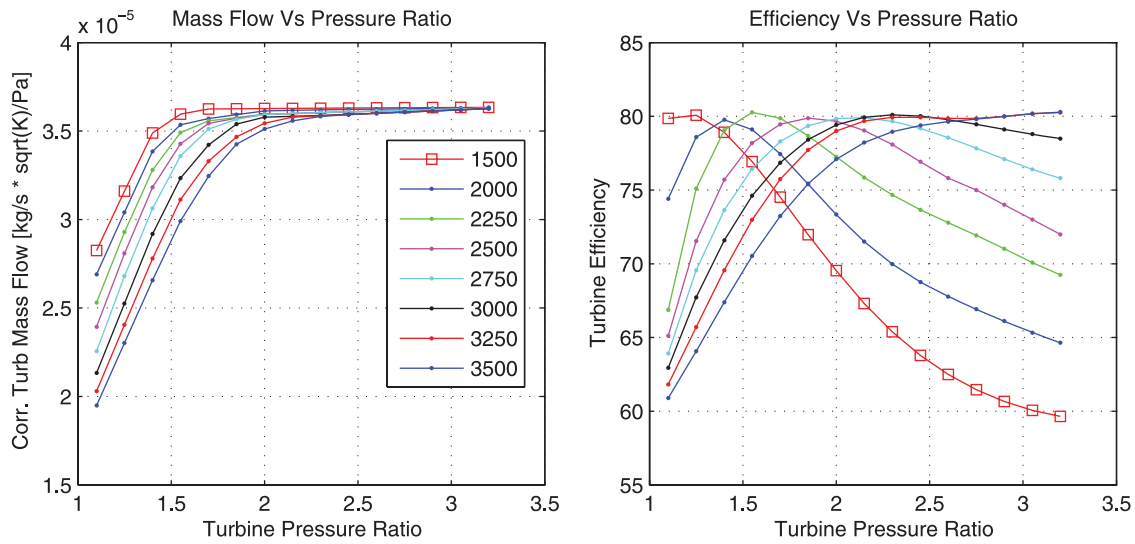

Fig. 3 Turbine map for the AMT Olympus engine

the temperature drop across the turbine is

$$\Delta T_{45} = \eta_t T_4 \left[1 - \left(\frac{P_5}{P_4} \right)^{(\gamma-1)/\gamma} \right] \tag{13}$$

The turbine exit temperature is therefore

$$T_5 = T_4 - \Delta T_{45} \tag{14}$$

and the torque generated by the turbine at a given rotational speed is expressed as

$$\tau_{\text{turb}} = \frac{w_t c_p \Delta T_{45}}{N_{\text{rad/s}}} \tag{15}$$

It should be noted that the turbine and compressor speeds are taken as equal since they are connected on a common shaft. The turbine exit conditions (w_5, T_5, P_5) are now established.

2.5 The AMT Olympus convergent nozzle

The ambient pressure outside the nozzle is taken as p_0, and the nozzle pressure ratio is hence

$$(P_r)_{\text{noz}} = \frac{P_5}{p_0} \tag{16}$$

The pressure ratio for which the nozzle exit speed reaches the speed of sound is called the critical pressure ratio and is a sole function of ratio of specific heat [**12**]

$$(P_r)_{\text{crit}} = \left(\frac{2}{1+\gamma} \right)^{\gamma/(1-\gamma)} \tag{17}$$

If the nozzle pressure ratio $(P_r)_{\text{noz}}$ is greater than $(P_r)_{\text{crit}}$, the nozzle will choke and the nozzle pressure ratio will be limited to $(P_r)_{\text{crit}}$. For a convergent nozzle with exit area (A_n), the mass flow through the nozzle is given by the following expression from reference [**12**]

$$w_n = \frac{A_n P_5}{R} (P_r)^{-1/\gamma} \sqrt{\frac{2gc_p}{T_5}(1 - P_r^{-R/c_p})} \tag{18}$$

where P_r is the limited value of nozzle pressure ratio which is less than or equal to the critical pressure ratio $(P_r)_{\text{crit}}$. The nozzle jet velocity is a function of nozzle pressure ratio and total nozzle temperature

$$V_{\text{jet}} = \sqrt{2gc_p T_5 (1 - P_r^{-R/c_p})} \tag{19}$$

The net thrust is a sum of momentum and pressure components

$$F = w_n(V_{\text{jet}} - V_0) + A_n(P_6 - p_0) \tag{20}$$

where V_0 is the aircraft speed and P_6 is the pressure at the face of nozzle exit.

2.6 Evaluation of pressure derivatives: $\dot{P}_3$, $\dot{P}_5$

Figure 4 shows two control volumes for the AMT Olympus single-spool turbojet. The first control volume is associated between the compressor and combustor. The mass storage in this volume is used to calculate rate of change of compressor exit pressure ($\dot{P}_3$). The second control volume is between the turbine and nozzle and shall provide derivative of turbine exit pressure ($\dot{P}_5$). For the volume associated with the combustor chamber and the compressor, the rate of accumulation of mass is

$$\dot{m}_3 = w_3 + w_f - w_t \tag{21}$$

and similarly for the volume between the turbine and the nozzle, the rate of change of mass is

$$\dot{m}_5 = w_t - w_n \tag{22}$$

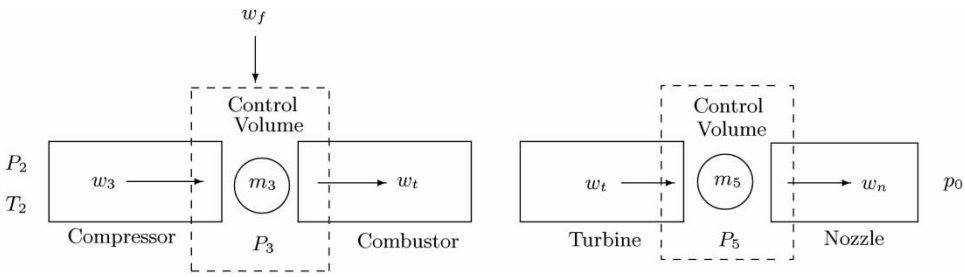

Fig. 4 Control volumes on a single-spool turbojet

Taking the time derivative of the ideal gas law and neglecting the temperature derivative term ($\dot{m}T$), as suggested by Fawke [**4**], gives

$$\dot{P} = \frac{RT}{V}(\dot{m}) \tag{23}$$

which was used to calculate the pressure derivatives ($\dot{P}_3, \dot{P}_5$), inside each control volume.

2.7 Evaluation of rotational acceleration ($\dot{N}$)

The rotational acceleration derivative ($\dot{N}$) is evaluated by calculating the difference in torque generated by the turbine and that required by the compressor

$$\dot{N} = \frac{\mathrm{d}N}{\mathrm{d}t} = \frac{\eta_{\mathrm{m}}\tau_{\mathrm{turb}} - \tau_{\mathrm{comp}}}{I_{\mathrm{spool}}} \tag{24}$$

This expression was integrated to get shaft rotational speed as a function of time. Using the above formulation, a dynamic model for the AMT Olympus engine was implemented in MATLAB/Simulink and is shown in Fig. 5.

2.8 Engine speed controller

To run the engine simulation model and test various bleed cases at different throttle settings an engine speed control system was designed. The control scheme is shown in Fig. 6. The controller uses a proportional + integral architecture, with the maximum fuel limit set by either the maximum allowable fuel flow or the turbine entry temperature (TET), T_4. An anti-windup was used for the integral element and the input engine speed demand was slew rate limited for

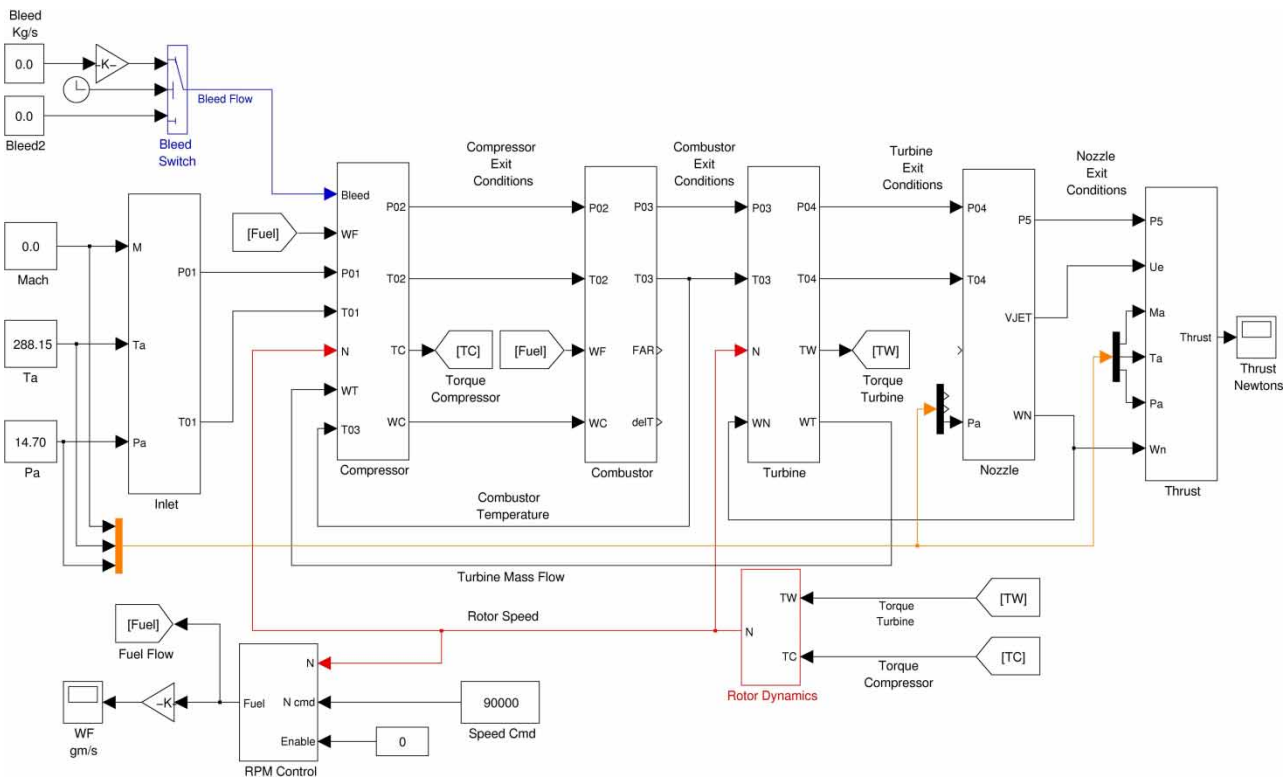

Fig. 5 Simulink model for AMT Olympus turbojet with bleed flow input

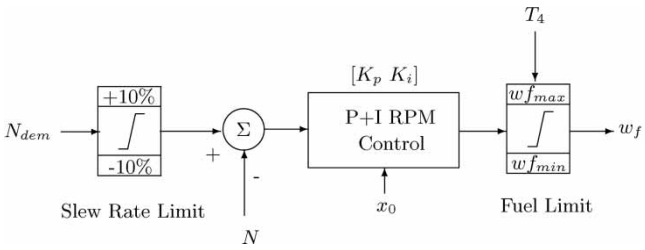

Fig. 6 Engine speed control system architecture

both engine acceleration and deceleration. The slew rate limit was set to ±10 per cent of the maximum engine speed. Gain values for the proportional and integral were set at $K_\mathrm{p} = 0.05$ and $K_\mathrm{i} = 0.0075$, respectively. The initial integral state (x_0) in the engine speed controller was set to 50 per cent of maximum fuel flowrate.

3 AMT OLYMPUS TURBOJET ENGINE

The simulation method described previously was validated on the AMT Olympus [**6**] turbojet engine (Fig. 7). It is a small engine that generates up to 190 N of thrust. The engine has a single-stage centrifugal compressor and single-stage axial turbine. The combustor chamber is of annular type. An electronic engine control unit (ECU) controls the revolutions per minute and limits the maximum exhaust gas temperature (EGT). The basic engine specifications as derived from reference [**6**] are shown in Table 1.

Besides the component map data, certain other engine parameters were required to complete the engine model. These were adjusted to match the experimental results. A combustion burner efficiency of 0.88 was used, together with combustion chamber pressure loss of 5 per cent. The intake and mechanical transmission efficiencies were set at 1.0 and 0.92, respectively. A rotor inertia of 0.0004 kg m^2 was assumed. An exact value of rotor inertia was not available, so this was adjusted by observing the time to reach maximum revolutions per minute. An effective nozzle area which is 95 per cent of the geometrical nozzle area was used to cater for the effect of boundary layer growth in the nozzle. Two control volumes were needed to calculate the pressure derivatives; these were selected as 1.0 and 0.75 ft^3 for the volumes associated with compressor/combustor and turbine/nozzle, respectively. The initial state vector was set at

$$\boldsymbol{X}_0 = [P_3, P_5, N] = [2.2P_2, 1.5P_2, 88\,000] \tag{25}$$

which places the engine operating point at a reasonable location on the compressor and turbine maps.

Table 1 Technical data AMT Olympus

Engine parameter	Value
Diameter (mm)	130
Length (mm)	270
Maximum thrust (N)	190
Pressure ratio	4:1
Mass flow (kg/s)	0.4
Maximum rotational speed (r/min)	112 500
Nominal EGT (K)	923
Maximum EGT (K)	973
Maximum fuel consumption (kg/min)	0.4

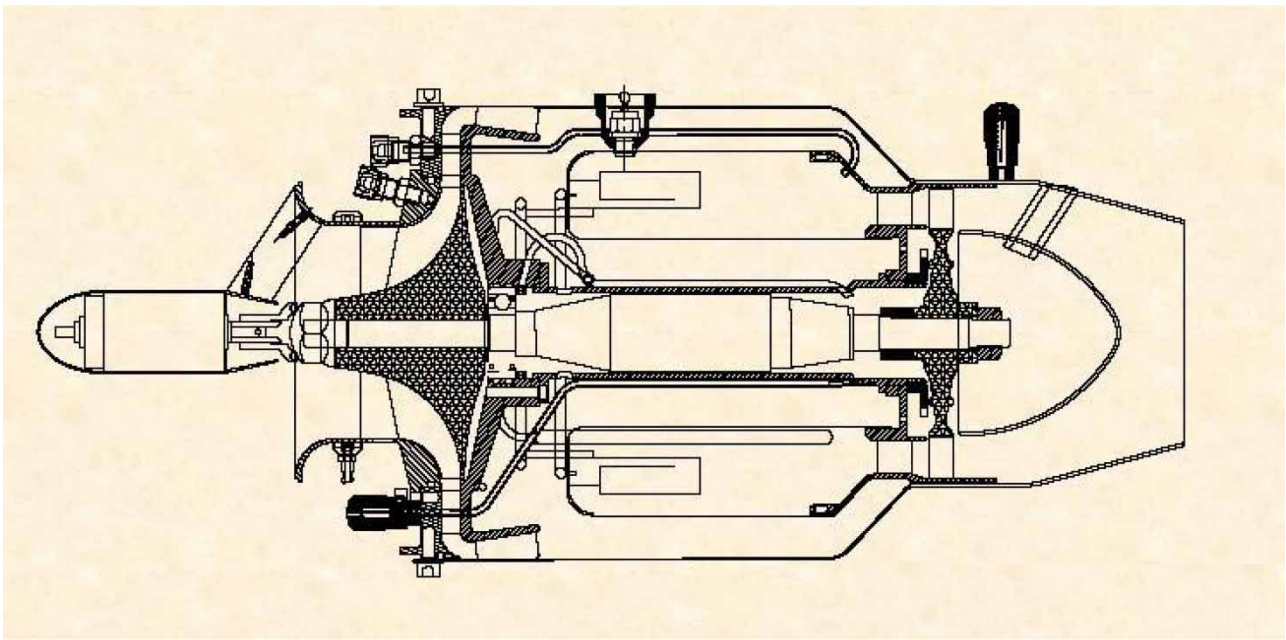

Fig. 7 AMT Olympus single-spool turbojet engine [**10**]

4 SIMULATION DESCRIPTION

The engine simulation can be divided into two parts: pretransient phase and the transient

4.1 Pretransient

Keeping a fixed value of fuel inflow, the simulation runs till it reaches a state when $\dot{\boldsymbol{X}} = 0$ and there is no accumulation of mass in any control volume. This phase is called the pretransient and with the control vector $\boldsymbol{u} = [w_f, A_n]$ fixed, the simulation converges to a steady-state condition. The pretransient phase can be avoided by using the last known converged or steady-state values of $\boldsymbol{X}_0$ and control input ($\boldsymbol{u}_0$), respectively. In Fig. 8, the line from point A to B shows the path followed by the engine as it settles down to a steady-state condition in the pretransient phase. Point A represents the initial condition, $\boldsymbol{X}_0$, on the compressor map as specified at start of the simulation and point B corresponds to a steady-state condition reached, according to the fuel setting specified in $\boldsymbol{u}_0$.

4.2 Transient

Once the engine has reached a steady-state condition at point B, the control vector $\boldsymbol{u} = [w_f, A_n]$ consisting of fuel flowrate and nozzle area can be varied to initiate a transient. During a transient, it takes a finite amount of time for the rotor to spool up or down but the mass flow and therefore pressure changes inside the engine can be quite rapid. The effect of a sudden increase in fuel flow is to move the compressor operating point up along the speed line towards surge. A sudden reduction in fuel flow causes the reverse action and the compressor operating point moves down towards the choking point. Path B to C in Fig. 8, shows the transient response of the AMT Olympus engine to a slew rate limited engine speed demand. The transient was run with engine speed control engaged. The engine settles down at point C corresponding to maximum speed demand of 112 500 r/min.

5 SIMULATION RESULTS AND VALIDATION

5.1 Steady-state results

The steady-state experimental values under zero compressor bleed were compared at maximum speed with engine speed control engaged. Values of fuel flow, thrust, compressor pressure ratio, and mass flow were noted. Table 2, summarizes the steady-state results at maximum engine speed.

It is evident that there is a good match between the experimental and the simulated values. The percentage errors are less than 3 per cent for most of the parameters except the EGT error, which is approximately 6 per cent. The simulation predicts lesser values of EGT at maximum engine speed. However, as will be discussed later, at lower engine speed values, the EGT correlation was much better.

Table 2 AMT Olympus engine steady state comparison at 112 500 r/min

Engine parameter	Experimental	Simulated	Percentage error
Maximum thrust (N)	193	189.5	+1.81
Pressure ratio	3.55	3.47	+2.25
Maximum fuel (gm/s)	9.10	8.85	+2.75
EGT (K)	1035	970	+6.28

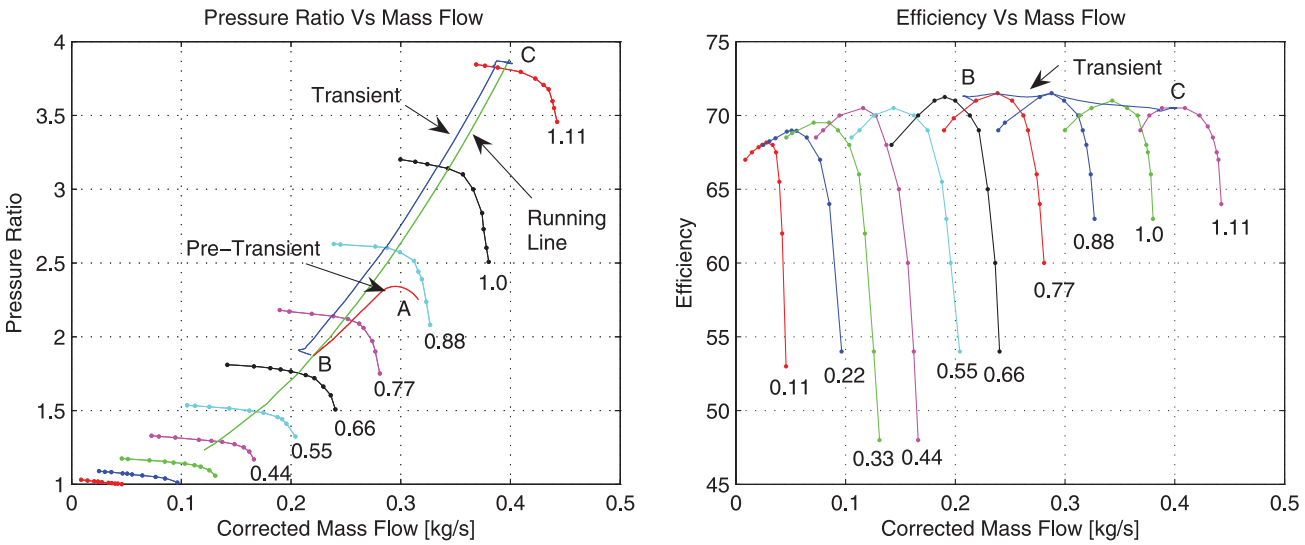

Fig. 8 Transient and pre-transient on the AMT Olympus compressor map

Figure 9 shows a correlation between static experimental and simulated engine thrust as a function of engine speed. Besides the engine setting, various environmental factors affect engine thrust. A higher ambient temperature results in a drop in thrust and rise in EGT while a lower ambient pressure results in a loss in the compressor delivery pressure and thrust. The mean static correlation for thrust under zero bleed conditions was within 5 per cent of experimental values. The engine mechanical transmission efficiency was adjusted from 0.99 to 0.92 to match the EGT values of the experiments. With higher mechanical efficiency the simulation predicted lower values of EGT. From Fig. 9, the EGT correlation is quite good at lower speeds but degrades at higher engine speeds, suggesting that the mechanical efficiency (η_m) may not be constant over the whole engine speed range. The fuel burning efficiency was decreased from 0.98 to 0.88 to match the excessive fuel consumed by the engine. This could also be attributed to the fact that the manufacturer uses 5 per cent oil in the fuel for lubrication purposes [**6**] and a relatively simple combustor model was used. The fuel consumption as function of engine speed as well as compressor exit pressure is also presented in Fig. 9.

5.2 Bleed experimentation

The bleed experiments [**7**] were conducted at the University of Manchester's Jet Engine Test Facility. These experiments were done as a part of flapless aerial vehicle integrated interdisciplinary research project, which aims at developing novel technologies for control of future aircraft. The bleed air was extracted from 30 radially symmetric holes on the AMT Olympus engine's centrifugal compressor. The amount of bleed was controlled by a bleed valve and various engine parameters were recorded by a data acquisition system. At a given throttle setting, as the amount of

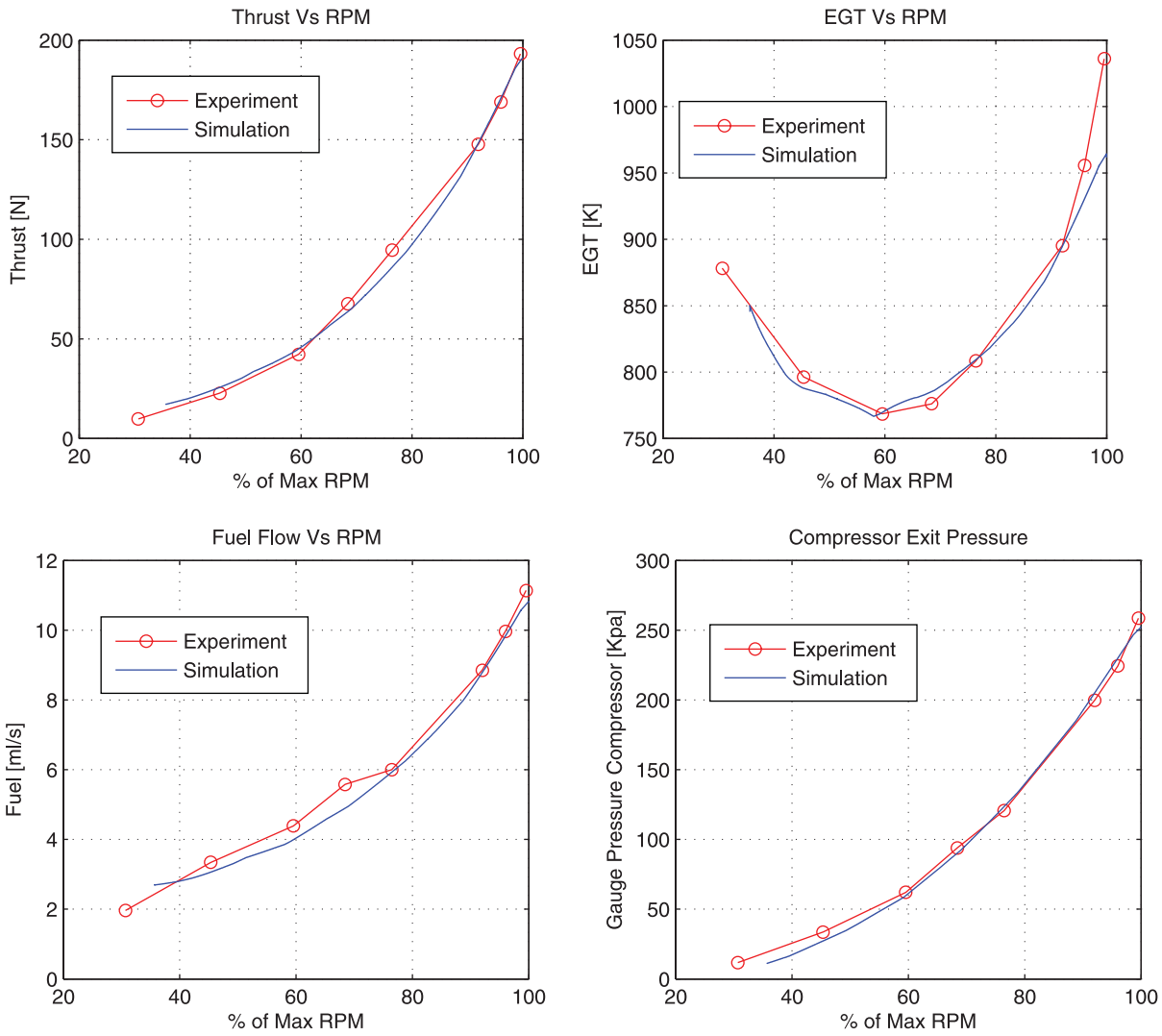

Fig. 9 AMT Olympus steady-state results: thrust, EGT, fuel, and compressor exit pressure

bleed is varied the electronic engine control adjusts the fuel flow in an attempt to keep the revolutions per minute constant. However, in nearly all bleed cases, the EGT limit is hit as the bleed reaches approximately 30 per cent of compressor mass flow. This bleed air from the engine is used to power (a) a circulation control actuator and (b) a fluidic thrust vectoring system [**7**]. Experimental testing was considered necessary to quantify the effect of engine bleed on its performance and to identify the boundaries of safe engine operation.

5.3 Bleed simulation and validation

Bleed extraction from the compressor has a degrading effect on engine performance. It alters the work and mass flow balance on engine components. Pilidis and Palmer [**13**] state that upon bleed extraction the turbine will have to operate with a lower mass flow to produce the work required by the compressor. This will result in a higher TET (T_4) and therefore higher EGT (T_5). The turbine is designed to operate choked even at relatively reduced mass flows, and therefore the non-dimensional mass flow ($w_t\sqrt{T_4}/P_4$) through the turbine is constant. To keep the non-dimensional mass flow constant, the turbine entry pressure P_4 will drop. This implies that compressor pressure ratio will fall. The steady-state running line will shift towards choke with a corresponding reduction in compressor efficiency. Pilidis and Palmer [**13**] suggest that when the non-dimensional bleed (ϕ) is small, the decrease in compressor pressure ratio due to bleed extraction can be approximated as

$$\left(\frac{P_3}{P_2}\right)_{\text{bleed}} \approx \left(\frac{P_3}{P_2}\right)_{\text{no 1bleed}} \sqrt{1-\phi} \tag{26}$$

and the corresponding increase in TET T_4 is

$$(T_4)_{\text{bleed}} = (T_4)_{\text{no bleed}} \frac{1}{1-\phi} \tag{27}$$

Bleed simulation was performed using the engine simulation program and compared with experimental results. Four throttle settings were simulated: 40, 53, 61, and 76 per cent. The input for the bleed simulation is the actual experimental fuel and bleed flowrates. This sets the engine operating point. Once the engine reaches a steady state for a given fuel and bleed flow, the input is changed to the next value. In this way, all the bleed cases were tested in a single-simulation run.

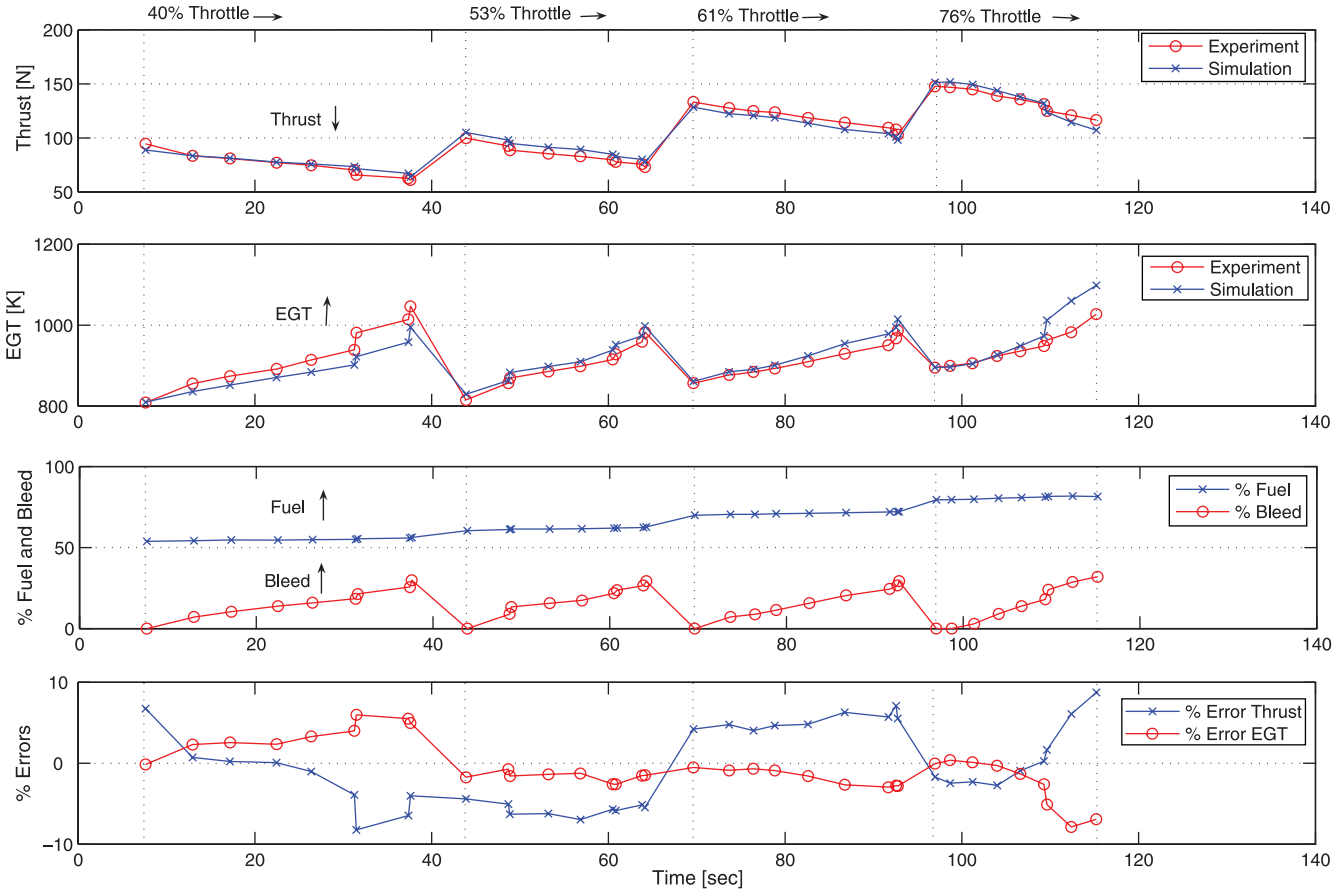

Fig. 10 Bleed simulation – drop in thrust due to bleed at different throttle settings

Table 3 Validation of bleed results: 61 per cent throttle setting

Net mass flow (gm/s)	Percentage bleed	Fuel flow (gm/s)	Thrust (N)			EGT (K)		
			Experimental	Simulated	Percentage error	Experimental	Simulated	Percentage error
336.29	0.00	6.36	133.17	127.57	+4.2	856.5	861.0	−0.5
347.75	7.17	6.41	127.57	121.49	+4.8	877.1	884.9	−0.9
350.05	8.79	6.41	124.79	119.78	+4.0	884.4	890.6	−0.7
354.68	11.29	6.44	123.67	117.91	+4.7	892.9	901.0	−0.9
359.50	15.64	6.47	118.56	112.87	+4.8	909.4	923.9	−1.6
363.92	20.39	6.51	114.18	107.01	+6.3	929.4	954.3	−2.7
370.47	24.33	6.55	109.38	103.14	+5.7	950.2	978.3	−3.0
372.60	26.47	6.56	108.00	100.37	+7.1	967.3	994.1	−2.8
374.95	29.13	6.56	103.05	97.37	+5.5	986.7	1014.6	−2.8

Figure 10 shows that as the bleed flow is increased, the thrust decreases and the EGT increases. Even at lower throttle settings, as the bleed flow is increased, the EGT hits the upper limit. At this point, the fuel or bleed flow cannot be increased further. Hence there is an upper limit on the amount of bleed that can be extracted at any given throttle setting or engine revolutions per minute. The percentage errors for thrust and EGT are within 5–10 per cent of experimental values. This variation is expected since the compressor characteristics change with the amount of bleed flow, and only steady-state compressor maps under no bleed conditions were used for the simulation. It may also be noted that as the engine bleed is increased the electronic ECU tries to adjust the corresponding drop in speed by increasing the value of fuel flow. Each step in the fuel flow setting corresponds to a different value of throttle setting. Table 3 summarizes the experimental and simulated results for the 61 per cent throttle case.

6 CONCLUSIONS

A gas turbine simulation program was written in MATLAB/Simulink environment and performance was compared with experimental values. The results were accurate to within 5 per cent for the nominal or zero bleed case and within 10 per cent for excessive bleed cases. The increase in error upon bleed extraction can be attributed to two factors. First, the location where the bleed is extracted affects the amount of work required by the compressor and this may also vary non-linearly for the radial compressor of the AMT Olympus engine. Second, the bleed extraction itself may adversely influence the performance of the compressor and the compressor characteristics may change. Further work will be required to more accurately model the compressor map with bleed extraction and improve upon the accuracy of the overall simulation. It may be noted here that the compressor/turbine maps have been derived from reference [**10**] and the experimental data from reference [**7**]. Although both sources refer to the same AMT Olympus engine, the possibility of statistical variation between the available component maps and the actual engine under test exists. It is possible to further adjust the component efficiencies in order to match the experimental results, however, this was not done in this case. This simulation method runs in real time and therefore can easily be integrated with aircraft and active flow control simulation codes.

ACKNOWLEDGEMENTS

The authors would like to extend their acknowledgements to Dr Crowther and his research team at the University of Manchester for the experimental data of the AMT Olympus engine. These data were subsequently used for simulation validation.

REFERENCES

1 **Leibeck, R. H.** Design of the blended wing body subsonic transport. *J. Aircr.*, 2004, **41**(1), 10–25.
2 **Latunia, G. P.** Active control of flow separation from the slat shoulder of a supercritical airfoil. In the 1st Flow Control Conference, St Louis, Missouri, 24–26 June 2002, AIAA paper 2002-3156.
3 **Englar, R. J.** Development of circulation control technology for application to advanced subsonic transport aircraft. *J. Aircr.*, 1994, **31**, 1160–1177.
4 **Fawke, A. J.** *Digital computer simulation of gas turbine dynamic behaviour*. PhD Thesis, University of Bristol, Bristol, UK, 1970.
5 **Parker, K.** and **Guo, T. H.** Development of turbofan engine simulation in a graphical simulation environment, NASA TM 2003-212543, 2003.
6 AMT Engine Documentation. AMT Olympus engine user's manual serial no 112171, Advanced Micro-Turbines (AMT), The Netherlands.
7 **Gill, K., Wilde, P., Gueroult, R.,** and **Crowther, W. J.** Development of an integrated propulsion and pneumatic power supply system for flapless UAVs. In the AIAA Aviation Technology, Integration and Operations Conference, Belfast, UK, 18–20 September 2007, AIAA paper 2007-7726.

8 Cohen, H., Rogers, G. F. C., and **Saravanamuttoo, H. I. H.** *Gas turbine theory,* 1996 (Addison Wesley Longman Ltd, Harlow).

9 Daughtery, R. L. *Fluid mechanics with engineering applications*, 1997 (McGraw Hill, New York).

10 Lichtsinder, M. and **Levy, Y.** Jet engine model for control and real time simulations. *J. Eng. Gas Turbine Power*, 2006, **128**, 745–753.

11 Walsh, P. P. and **Fletcher, P.** *Gas turbine performance*, 1999 (Blackwell Science Ltd, Oxford).

12 Mattingly, J. D. *Elements of gas turbine propulsion,* 1996 (McGraw Hill, New York).

13 Pilidis, P. and **Palmer, J. R.**, Gas turbine theory and performance. MSc Thermal Power Course Notes, 2006.

APPENDIX

Notation

A_n	nozzle exit area
c_p	specific heat at constant pressure
I_{spool}	rotational inertia of spool
K_i	revolutions per minute controller integral gain
K_p	revolutions per minute controller proportional gain
l	length of the compressor
$\dot{m}_3$	mass storage rate in compressor-combustor volume
$\dot{m}_5$	mass storage rate in turbine-nozzle volume
N	shaft rotational speed in revolutions per minute
N_{dem}	shaft speed demand
N_c^*	corrected compressor speed
N_t^*	corrected turbine speed
p_0	ambient pressure
P_{std}	standard pressure at sea level
P_1	total pressure at diffuser inlet
P_2	total pressure at compressor inlet
P_3	total pressure at combustor inlet
P_4	total pressure at turbine inlet
P_5	total pressure at nozzle inlet
ΔP_{loss}	pressure loss in combustion chamber
R	gas constant
t_0	ambient temperature
T_{std}	standard temperature at sea level
T_1	total temperature at diffuser inlet
T_2	total temperature at compressor inlet
T_3	total temperature at combustor inlet
T_4	total temperature at turbine inlet
T_5	total temperature at nozzle inlet
ΔT_{23}	temperature rise across compressor
ΔT_{34}	temperature rise across combustion chamber
ΔT_{45}	temperature drop across turbine
$\boldsymbol{u}$	control vector
V	inter-component volume
w_b	bleed mass flow
w_c	actual mass flow through compressor
w_{cool}	cooling bleed into turbine
w_f	mass flow of fuel
w_i	mass flow at station number i
w_n	nozzle mass flow
w_c^*	corrected mass flow through compressor
w_t	actual mass flow through turbine
w_t^*	corrected mass flow through turbine
x	bleed location along compressor length
x_0	initial state of the revolutions per minute control integral element
$\boldsymbol{X}$	state vector
γ	ratio of specific heats
η_b	combustor burning efficiency
η_c	compressor isentropic efficiency
η_I	intake efficiency
η_m	mechanical transmission efficiency
η_t	turbine isentropic efficiency
τ_{comp}	torque required by the compressor
τ_{turb}	torque generated by the turbine
ϕ	bleed fraction from compressor mass flow (w_b/w_c)